

## SUPPORTING INFORMATION

### **Direct photoisomerization of CH<sub>2</sub>I<sub>2</sub> vs CHBr<sub>3</sub> in the gas phase: a joint 50 fs experimental and multireference resonance-theoretical study**

Veniamin A. Borin, Sergey M. Matveev, Darya S. Budkina, Patrick Z. El-Khoury,<sup>1</sup> Alexander N.  
Tarnovsky\*

*Department of Chemistry and Center for Photochemical Sciences, Bowling Green State  
University, Bowling Green, OH, 43402, USA*

<sup>1</sup>Present address: Physical Sciences Division, Pacific Northwest National Laboratory, P.O. Box  
999, Richland, WA 99352, USA

#### **CONTENTS:**

I. Spectroscopy of CH <sub>2</sub> I <sub>2</sub> and CHBr <sub>3</sub> : A Brief Summary	S2
II. Ultrafast Transient Absorption, Fig. 1S-4S	S3
III. Computational Background	S7
IV. Computational Results: Tables 1S-7S	S10
V. Computational Results: Fig. 5S-8S	S16
VI. References	S20

### Spectroscopy of $\text{CH}_2\text{I}_2$ and $\text{CHBr}_3$ : A Brief Summary

The UV absorption spectrum of  $\text{CHBr}_3$  is dominated by the  $\tilde{X}^1A_1 \rightarrow \tilde{B}^1E$  transition at  $\sim 220$  nm, whereas the lowest-energy singlet-singlet  $\tilde{X}^1A_1 \rightarrow \tilde{A}^1A_2$  transition is at 243 nm,<sup>1</sup> Fig. 1S. Previous works suggested a unity quantum yield for the Br-atom dissociation channel upon 248 nm excitation.<sup>2</sup> This is in disagreement with several other studies suggesting photoelimination of both molecular and atomic bromine,<sup>3-6</sup> where most of the Br atoms are produced in the ground  $^2P_{3/2}$  state.<sup>3,7</sup>

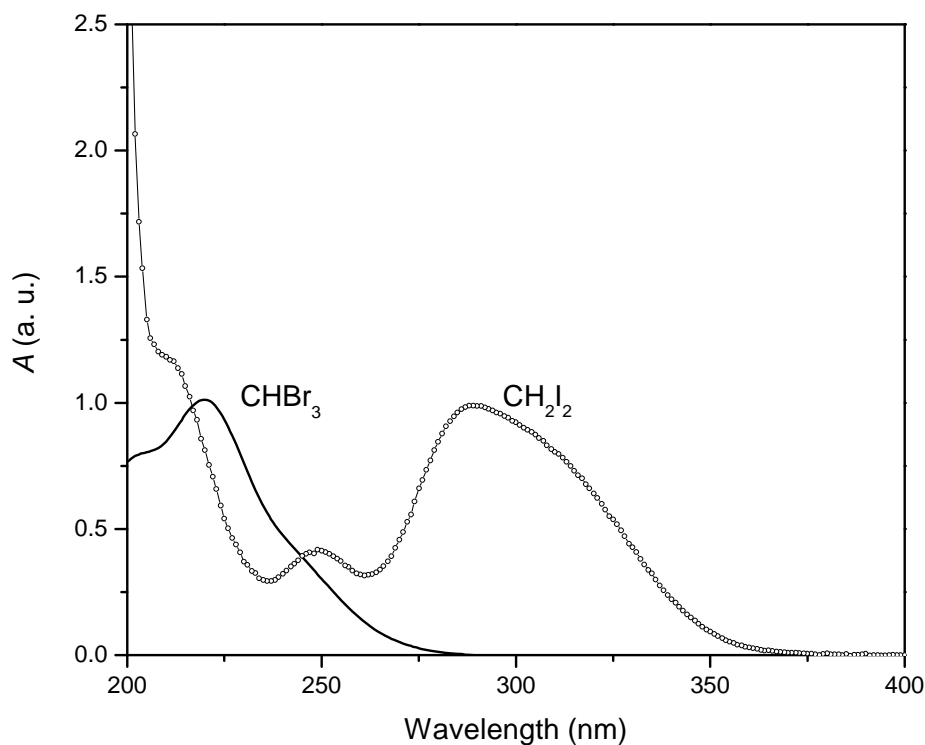


**Fig. 1S.** Steady-state absorption spectra of  $\text{CHBr}_3$  and  $\text{CH}_2\text{I}_2$  vapour.

For  $\text{CH}_2\text{I}_2$  at 330 nm, only the lowest singlet excited state is reached via the  $1^1A_1 \rightarrow 1^1B_1$  transition,<sup>8-11</sup> Fig. 1S.  $\text{CH}_2\text{I}_2$  in the  $1^1B_1$  state dissociates exclusively yielding  $\text{CH}_2\text{I}$  radicals and ground-state  $\text{I}(^2P_{3/2})$  iodine atoms.<sup>11-16</sup> Spin-orbit excited  $\text{I}^*(^2P_{1/2})$  photofragments observed in small quantum yields (from 3 to 7% upon 333 and 329 nm excitation, respectively)<sup>13,14</sup> are attributed to curve crossing with other electronic states of  $\text{CH}_2\text{I}_2$ . The  $\text{I}^*(^2P_{1/2})$  yield increases as the wavelength decreases.<sup>13,14,16</sup> Previous photofragment spectroscopy works showed that the dissociation in the low-lying excited states occurs on a time scale faster than the  $\text{CH}_2\text{I}_2$  rotational period,<sup>8</sup> i.e., ca. 10 ps.<sup>17</sup> The low-lying excited states of  $\text{CH}_2\text{I}_2$  computed along a single coordinate (the C–I bond length) are repulsive,<sup>18,19</sup> supporting the commonly adopted premise

that the only primary photochemical channel is direct dissociation of the C-I bond with the formation of the  $\text{CH}_2\text{I}$  and I fragments.

### *Ultrafast Transient Absorption*

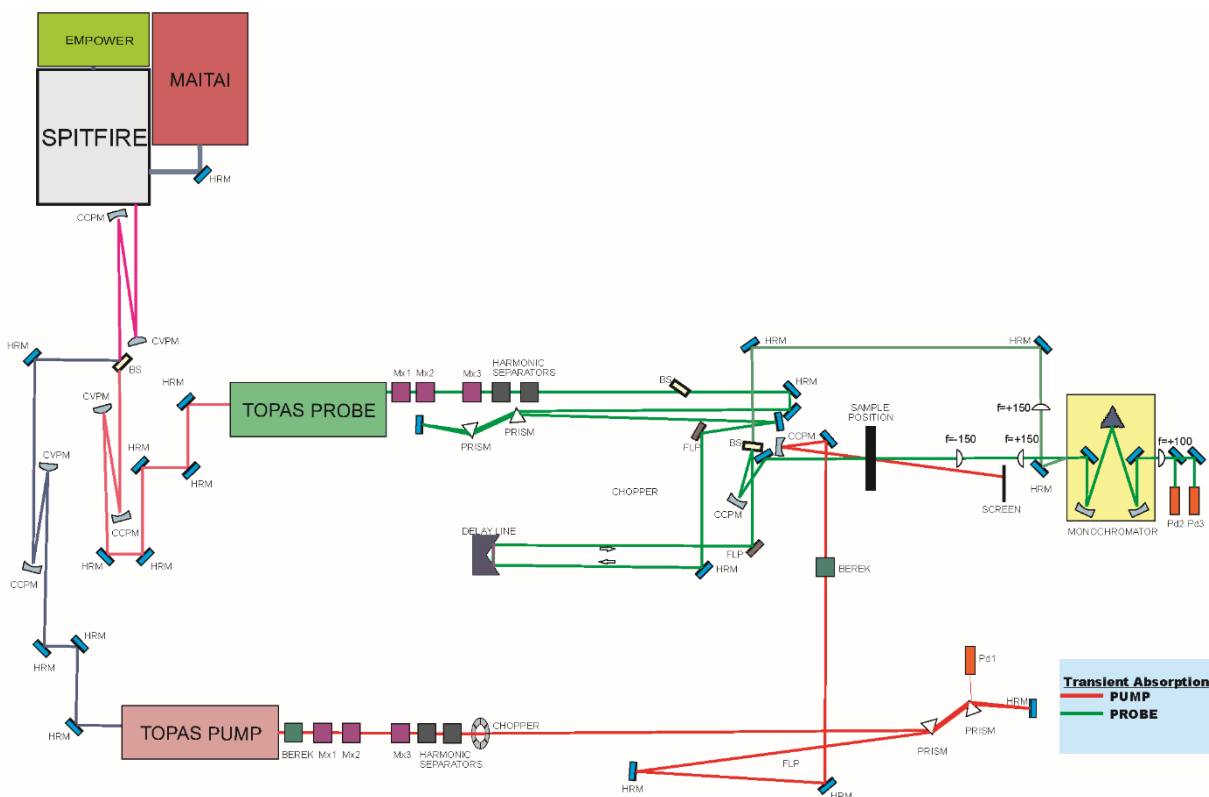


**Fig. 2S.** Schematic diagram of the experimental set-up used for the 40-fs time-resolved two-colour transient absorption measurements.

The transient absorption spectrometer is based on a Ti:Sapphire regenerative amplifier (Spitfire Pro, Spectra-Physics, 1kHz) that generates 35 fs (fwhm) 3.8 mJ pulses centered at 800 nm. The amplified output is split and used for pumping of two optical parametric amplifiers (TOPAS-C, Light Conversion Ltd.). One of the TOPAS-C (‘pump’) is set to produce deep-UV/UV pulses, which are sent through a calcium fluoride prism compressor for the correction of the phase dispersion and subsequently used for sample excitation. Another TOPAS-C (‘probe’) is set to generate much weaker visible pulses, which after the correction of their phase dispersion in a fused-silica-prism compressor are used for probing. Typical widths (fwhm = 40-50 fs) of a third-order correlation function measured via degenerative four-wave mixing of excitation and probe

pulses<sup>20</sup> indicate that the pulse duration is about 30-45 fs. A fraction of the probe beam is split off before the sample to be utilized as a reference for the correction of the shot-to-shot pulse-intensity fluctuations. The energy of the probe pulse passing through the sample and that of the reference pulse are detected by photodiodes and the photodiode signals are processed on a shot-to-shot basis by using a custom-made 1 kHz detection system (<http://www.pascherinstruments.com>). The absorbance change induced by excitation is evaluated by blocking every second excitation pulse with a mechanical chopper synchronized to the 1-kHz repetition rate of the amplified laser system.

To estimate the quantum yield of the isomer formation for the CH<sub>2</sub>I<sub>2</sub> vapour, the incident energy ( $E$ ), the energy after the sample ( $E_t$ ), and the transient absorption signal were measured under the identical 330-nm excitation (focusing) conditions in two different states: (i) for the vapour CH<sub>2</sub>I<sub>2</sub> sample, and immediately after this measurement, (ii) for the 100- $\mu$ m thick flowing liquid jet of CH<sub>2</sub>I<sub>2</sub> (solvents, acetonitrile and *n*-hexane) placed in the same position. For probing in the visible region, i.e., outside the absorption range of parent CH<sub>2</sub>I<sub>2</sub> molecules, the absolute quantum yield of the isomer formation is given by the following expression:<sup>21</sup>

$$\Phi_{iso} = \frac{\Delta A(\lambda_{pr})}{\varepsilon_{IS}(\lambda_{pr})} N_A 10^{-3} \frac{h\nu(\frac{\pi d^2}{4})}{E(1-10^{-A(\lambda_{exc})})} \quad (1)$$

Here,  $\Delta A(\lambda_{pr})$  is the transient absorption signal at a probe wavelength  $\lambda_{pr}$ ,  $\varepsilon(\lambda_{pr})$  is the extinction coefficient of the isomer product at  $\lambda_{pr}$ ,  $E$  is the incident excitation energy,  $A(\lambda_{exc})$  is the sample absorbance at the excitation wavelength  $\lambda_{exc} = 330$  nm,  $N_A = 6.022 \cdot 10^{23}$  mol<sup>-1</sup> is the Avogadro number, and  $d$  is the “equivalent diameter” of the excitation beam at the sample position. In eq. (1),  $E(1 - 10^{-A(\lambda_{exc})}) = E_a$ , which is the amount the energy absorbed by the sample over the distance of pump-probe beam overlap (measured to be 8 mm in the vapour, 100  $\mu$ m in the jet). In solution,  $E_a = E - E_t$ , and we obtained similar estimates of  $E_a$  based on  $A(330$  nm) known from the CH<sub>2</sub>I<sub>2</sub> UV absorbance. In the CH<sub>2</sub>I<sub>2</sub> vapour,  $E_a = E \left(1 - 10^{-A(\lambda_{exc})\frac{8}{25}}\right)$  taking into account the length of pump-probe overlap (8 mm) and the cell path length (25 mm). The ratio of the quantum yields of the isomer formation in the gas phase and in solution denoted as  $\Phi_{iso}^g$  and  $\Phi_{iso}^l$ , respectively, is given by:

$$\frac{\Phi_{iso}^g}{\Phi_{iso}^l} = \left[ \frac{\frac{\Delta A^g(\lambda_{pr})}{E_a^g}}{\frac{\Delta A^l(\lambda_{pr})}{E_a^l}} \right] \frac{\varepsilon_{IS}^l(\lambda_{pr})}{\varepsilon_{IS}^g(\lambda_{pr})} \quad (2)$$

For the typical values measured in the acetonitrile solution ( $\Delta A^l(380\text{ nm}) = 16\text{ mOD}$  in Fig. 3S,  $E_a^l = 0.17\text{ }\mu\text{J}$ ) and in the gas phase ( $\Delta A^g(384\text{ nm}) = 0.8\text{ mOD}$ ,  $E_a^g = 0.045\text{ }\mu\text{J}$ ), we obtain:

$$\frac{\Phi_{iso}^g}{\Phi_{iso}^l} = 0.19 \frac{\varepsilon_{IS}^l(\lambda_{pr})}{\varepsilon_{IS}^g(\lambda_{pr})} \quad (3)$$

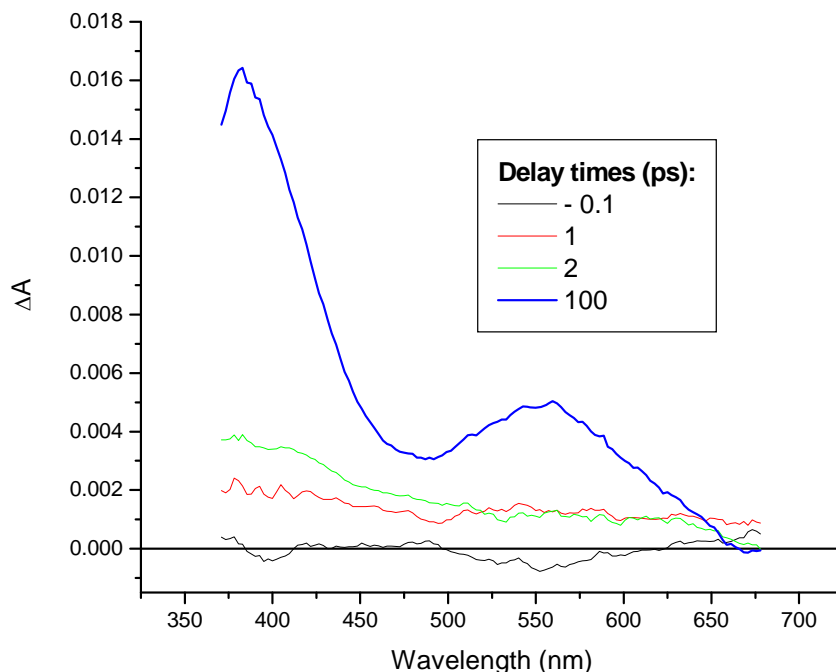


**Fig. 3S.** Transient absorption spectra of  $\text{CH}_2\text{I}_2$  in acetonitrile (0.4 M, 100- $\mu\text{m}$  jet) measured following 330 nm excitation ( $0.3\text{ }\mu\text{J pulse}^{-1}$ ). The  $\Delta A$  signal at 100 ps is due to the equilibrated isomer product species.<sup>22,23</sup>

The numerical factor in eq. (3) is the average of several measurements, including the measurements performed in *n*-hexane which yielded very close values, and its accuracy is evaluated to be  $\pm 0.051$ . The absolute quantum yield of *iso*- $\text{CH}_2\text{I}_2$  formation in acetonitrile was estimated to be  $0.69 \pm 0.15$  upon 266 nm excitation,<sup>22</sup> and  $1.00 \pm 0.30$  and  $0.71 \pm 0.21$  upon 310 and 350 nm excitation, respectively (unpublished data). The use of eq. (1) and  $d = 150\text{ }\mu\text{m}$  yields  $\Phi_{iso}^l = 1.0$  for 330 nm excitation, Fig. 3S. The average over last three experiments (excitation into  $S_1$  and  $S_2$ ) yields  $\Phi_{iso}^l = \sim 0.9$ . Therefore,  $\Phi_{iso}^g = 0.17 \frac{\varepsilon_{IS}^l(\lambda_{pr})}{\varepsilon_{IS}^g(\lambda_{pr})}$ . The ratio of the extinction coefficients in eq. (3) is expected to be  $> 1$ . Nascent isomers of polyhalogenated alkanes on *en route* from the CI to the isomer minimum (see Fig. 4 in ref. [24]) exhibit significantly weakened

(a factor of  $\sim 2$ ) absorption strength due to electronic factors. In addition, nascent isomer product species are vibrationally excited and have their peak absorbance reduced because of the redistribution of absorption outside the spectral region in which the equilibrated species absorb, e.g., red wavelengths in Fig. 3S. In solution,  $\epsilon_{IS}^I(386\text{ nm}) = 5590\text{ M}^{-1}\text{ cm}^{-1}$  in acetonitrile and  $6860\text{ M}^{-1}\text{ cm}^{-1}$  in non-polar *n*-hexane were evaluated.<sup>22</sup> Therefore, the quantum yield of the isomer formation in the  $\text{CH}_2\text{I}_2$  vapour upon 330 nm excitation is estimated to be  $\sim 20\%$  (lower limit).

$\text{CH}_2\text{I}_2$  in the  $1^1B_1$  state dissociates exclusively yielding  $\text{CH}_2\text{I}$  radicals and ground-state  $\text{I}(^2P_{3/2})$  iodine atoms.<sup>11-16</sup> Spin-orbit excited  $\text{I}^*(^2P_{1/2})$  photofragments observed in small quantum yields (from 3 to 7% upon 333 and 329 nm excitation, respectively)<sup>13,14</sup> are attributed to curve crossing with other electronic states of  $\text{CH}_2\text{I}_2$ . To demonstrate that the main features of the dynamics observed (regions 1-4 in Fig. 1, main text) have nothing to do with an admixture of  $\text{I}^*$ -producing channels, we carried out the transient absorption experiments utilizing a 340-nm excitation wavelength (the quantum yield of  $\text{I}^*$  at 340.6 nm is zero<sup>13</sup>), Fig. 4S. The ratio of the two  $\Delta A$  peaks changed reflecting the different relative strength of the excited-state ( $1^1B_1$ ) and isomer product absorption, but the same features of the dynamics were observed, regions 1-4 in Fig. 4S.

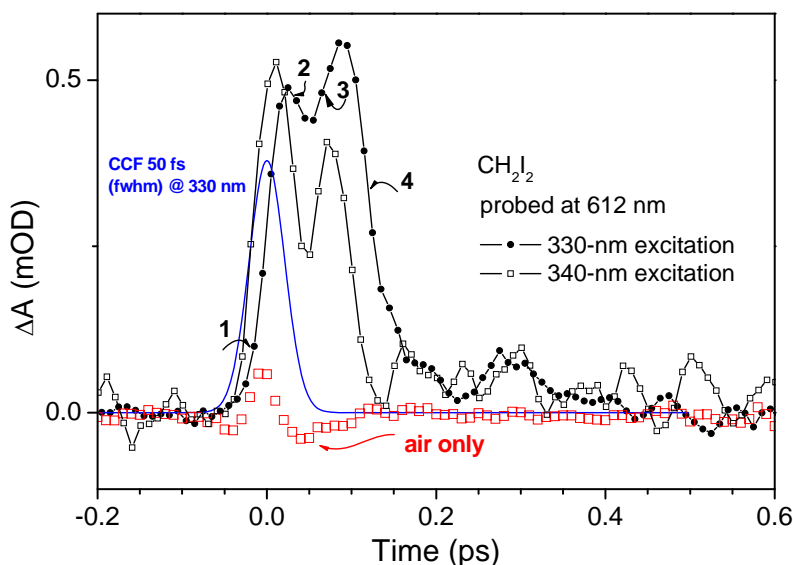


**Fig. 4S.** The comparison of the 330/612 nm transient absorption kinetic trace (Fig. 1, main text) and the 340/612 nm transient absorption kinetic trace measured for the  $\text{CH}_2\text{I}_2$  vapour. The same dynamic features (regions 1-4) are observed upon 330- and 340-nm excitation.

## ***Computational Background***

The description of excited electronic states generally requires a treatment of both static and dynamical electron correlation. The dynamic correlation is the result of instantaneous electron-electron repulsion. The static correlation is caused by state mixing, which is a typical situation where electronic states are near degeneracy, and in consequence, in none of the states involved the wavefunction can be described by a single Slater determinant. Popular methods such as Hartree-Fock, Møller-Plesset second-order perturbation theory (MP2), or Density Functional Theory (DFT) are single-configurational, meaning that they utilize a single Slater determinant for describing the wavefunction. This approximation is valid when electronic states do not come into close energetic proximity. For the description of the photoisomerization in  $\text{CHBr}_3$  because of the presence of the  $S_1/S_0$  surface crossing along the reaction path,<sup>25</sup> and in  $\text{CH}_2\text{I}_2$ , where the photoisomerization is similarly rapid and the presence of a conical intersection is suspected, this approximation cannot be expected to be valid. Furthermore, the isomer minimum is situated not far from radical dissociation asymptote. There are several computational methods accounting both for static and dynamic electron correlation. Among those, the method of choice is the multistate complete active space second order perturbation theory (MS-CASPT2), which is accurate, and at the same time, not prohibitively expensive. CASPT2 uses a linear combination of Slater determinants as a zero-order wavefunction (and therefore, it belongs to multireference methods<sup>26</sup>) and then performs energy and wavefunction corrections using perturbation theory. MS-CAPST2 has the electronic energy accuracy  $< 6.9$  kcal/mol in “almost all cases”,<sup>27,28</sup> making it “a true *gold standard*” for excited-state computational studies. MS-CASPT2, however, uses molecular orbital but not valence bond formalism. Yet, it is the latter that is useful for the description of fractional bonds and fractional charges developing in the course of a typical photochemical reaction. Despite the recent resurgence of the valence bond theory, we are not aware of any computational method that would use this language and yield correct energetics and structures for the molecules of interest. In computing resonance structures contributing to a given molecular geometry and their weights, Natural Resonance Theory (NRT) provides pictorially institutive structures showing bonding patterns and valence electrons that are not used in bonding. However, NRT is not compatible with CASPT2. A possible solution is single-point energy computation along the MS-CASPT2 MEP using a method (i) compatible with NRT, (ii) with accuracy not lower than that of MS-CASPT2. Advanced correlation methods, such as

EOM-CCSD<sup>29</sup> or CISD,<sup>30-32</sup> are single reference, and as a result, they fail in the proximity of CI.<sup>33</sup> Thus, we have chosen the multireference averaged coupled pair functional (MRACPF), which is a size-extensive version of MRCI (multireference configuration interaction).<sup>34</sup> MRACPF gives the energetics and wavefunction very similar to those of MS-CASPT2, according to our computations on CHBr<sub>3</sub> and CH<sub>2</sub>I<sub>2</sub>. But MRACPF is much more computationally expensive, and therefore, the use of MRACPF is unreasonable for MEP, but reasonable for single-point computations.

To support the data and conclusions given in the main manuscript text, we provide Figure 5S and 6S, which summarize the active space molecular orbitals of CHBr<sub>3</sub> and CH<sub>2</sub>I<sub>2</sub> used for the MS-CASPT2 calculations, the MS-CASPT2 optimized structures of CHBr<sub>3</sub> and *iso*-CHBr<sub>3</sub> (Table 1S) as well as CH<sub>2</sub>I<sub>2</sub> and *iso*-CH<sub>2</sub>I<sub>2</sub> (Table 2S), the structural parameters along the MS-CASPT2 MEP of CHBr<sub>3</sub> and CH<sub>2</sub>I<sub>2</sub> (Table 3S and 4S), and the list of previously considered resonance structures the contribution of which we found to be insignificant (Table 5S).

In addition, for CH<sub>2</sub>I<sub>2</sub> we provide the comparison of the geometrical parameters as well as vertical excitation energies computed using various basis sets within the MS-CASPT2 method (Table 8S), the effect of the use of a larger active space on the MEP (Fig.7S), and the effect of the inclusion of the spin-orbit coupling on the VETs (Table 7S) and on the MEP and (Fig. 8S).

Table 6S shows the comparison of the structural and spectroscopic parameters of the parent CH<sub>2</sub>I<sub>2</sub> molecule, obtained by using the MS-CASPT2 method with different basis sets, namely, 6-311G\*\*,<sup>35</sup> ANO-RCC-xZVP (x = D, T, and Q),<sup>36</sup> and using the EOM-CCSD<sup>29</sup> method with the 6-311G\*\* basis set. The last column in Table 6S gives the average computer time needed to perform a single point energy calculation. This value is important because it shows how computationally demanding is a certain computational method. The comparison with the experimental geometrical parameters and vertical excitation energies demonstrates that MS-CASPT2/6-311G\*\* is a reasonable trade-off between the accuracy and computational cost, and therefore, this method is used throughout this work. An increase of the active space to (16,12) does not significantly change the energy and topology of the photoisomerization path (Fig. 7S).

Previous spin-orbit coupling investigations<sup>18,19</sup> suggested that the low-energy electronic states have significant triplet character. In agreement with these studies, for the experimental excited state (<sup>1</sup>B<sub>1</sub>) of interest reached upon 330-nm excitation, we found a significant triplet character at the FC point. As one can see from Table 7S, on average between our and two



previous<sup>18,19</sup> spin-orbit studies, the probability to excite CH<sub>2</sub>I<sub>2</sub> into the strongest absorbing triplet state is ~17 times less likely than direct excitation of CH<sub>2</sub>I<sub>2</sub> into the lowest singlet 1<sup>1</sup>B<sub>1</sub> state (S<sub>1</sub>) at 330-nm photon energy. Inclusion of spin-orbit coupling at the MS-CASPT2/CASSI-SO level confirms the energy and topology of the MEP (Fig. 8S, MS-CASPT2/CASSI-SO/6-311G\*\*). Furthermore, similarly to the spin-free electronic states, the spin-coupled electronic states exhibit no crossing prior to the CI point. Implementation of the NRT analysis to spin-orbit-coupled states is currently impossible because the density matrices at present can only be generated for spin-free states. However, because the energy and topology of the photoisomerization process are nearly the same when described using the spin-free and spin-orbit coupled states, it is likely that the NRT analysis of spin-free singlet states yields the reliable result.

**Table 1S.** The MS-CASPT2 optimized structures of  $\text{CHBr}_3$  and *iso*- $\text{CHBr}_3$ . The interatomic distances are given in Å, and the angles in degrees. The migrating bromine is labelled as Br(2) and the bromine-bromine bond in *iso*- $\text{CHBr}_3$  is labelled as Br(2)–Br(3).

	C–H	C–Br(1)	C–Br(3)	C–Br(2)	Br(2)–Br(3)	H–C–Br(1)	Br(1)–C–Br(3)	C–Br(3)–Br(2)	H–C–Br(3)–Br(2)
$\text{CHBr}_3$	1.08	1.94	1.94	1.94	3.22	107.0	112.0	34.2	116.5
<i>iso</i> - $\text{CHBr}_3$	1.08	1.86	1.81	3.99	2.74	115.8	121.9	121.5	72.8

**Table 2S.** The MS-CASPT2 optimized structures of  $\text{CH}_2\text{I}_2$  and *iso*- $\text{CH}_2\text{I}_2$ . The interatomic distances are given in Å, and the angles in degrees.

	C–H	C–I(1)	C–I(2)	I(1)–I(2)	H–C–I(1)	C–I(1)–I(2)	H–C–I(1)–I(2)
$\text{CH}_2\text{I}_2$	1.08	2.16	2.16	3.66	107.4	32.2	119.8
<i>iso</i> - $\text{CH}_2\text{I}_2$	1.08	1.99	4.42	3.08	117.6	119.8	78.1

**Table 3S.** The structural parameters along the MS-CASPT2 MEP of  $\text{CHBr}_3$ . The first and eighth MEP points correspond to the optimized structure of  $\text{CHBr}_3$  and the structure of *iso*- $\text{CHBr}_3$ . The interatomic distances are given in Å, and the angles in degrees. The migrating bromine is labelled as Br(2) and the bromine-bromine bond in *iso*- $\text{CHBr}_3$  is labelled as Br(2)–Br(3).

MEP point	C–H	C–Br(1)	C–Br(3)	C–Br(2)	Br(2)–Br(3)	H–C–Br(1)	Br(1)–C–Br(3)	C–Br(3)–Br(2)	H–C–Br(3)–Br(2)
1	1.08	1.94	1.94	1.94	3.22	107.0	112.0	34.2	116.5
2	1.07	1.86	1.86	2.97	3.52	115.8	120.9	57.4	120.8
3	1.08	1.87	1.87	3.57	3.94	116.2	120.1	64.7	117.5
4	1.08	1.87	1.87	3.80	4.24	116.2	120.1	63.4	111.7
5	1.08	1.86	1.87	3.75	4.08	116.9	120.3	66.6	125.7
6	1.08	1.86	1.81	3.76	2.94	116.6	119.6	101.7	103
7	1.08	1.87	1.80	3.92	2.71	115.9	121.2	119.2	102.7
8	1.08	1.87	1.81	4.15	2.72	115.2	123.6	131.2	113.4

**Table 4S.** The structural parameters along the MS-CASPT2 MEP of CH<sub>2</sub>I<sub>2</sub>. The first and eighth MEP points correspond to the optimized structure of CH<sub>2</sub>I<sub>2</sub> and the structure of *iso*-CH<sub>2</sub>I<sub>2</sub>. The interatomic distances are given in Å, and the angles in degrees.

MEP step	C-H	C-I(1)	C-I(2)	I(1)-I(2)	H-C-I(1)	C-I(1)-I(2)	H-C-I(1)-I(2)
1	1.08	2.16	2.16	3.66	107.4	32.2	119.8
2	1.08	2.07	3.06	3.89	115.6	51.5	72.9
3	1.08	2.07	3.52	4.15	116.5	57.9	77.1
4	1.08	2.06	3.94	4.20	117.3	68.5	80.8
5	1.08	2.06	4.20	4.20	117.3	75.5	80.8
6	1.08	2.04	4.15	3.72	116.9	86.9	79.7
7	1.08	2.00	4.10	3.26	117.2	99.7	78.7
8	1.08	1.99	4.34	3.08	117.4	116.1	78.2
9	1.08	2.01	4.68	3.10	118.0	131.0	78.6

**Table 5S.** Selected resonance structures (X = Br or I), including those previously considered for the *iso*-CH<sub>2</sub>I<sub>2</sub> and *iso*-CHBr<sub>3</sub> species by Maier, Reid and co-workers,<sup>37-42</sup> the contribution of which we found to be insignificant all throughout the computed MEP (<5%).

Resonance structures	<i>iso</i> -CHBr <sub>3</sub>	<i>iso</i> -CH <sub>2</sub> I <sub>2</sub>
Three-body dissociation species		
Radical species produced via H-atom dissociation		
Carbene-dihalogen complex		
Three-center four-electron hypervalent		
Open-shell singlet born out from a halide-halocarbenium contact ion pair by decoupling the C-X double bond		
Contact ion pair with a positive charge on the carbon atom and a negative charge on the outer X atom		

**Table 6S.** Performance of various basis sets with the MS-CASPT2 level of theory and the EOM-CCSD method applied to the CH<sub>2</sub>I<sub>2</sub> parent molecule.

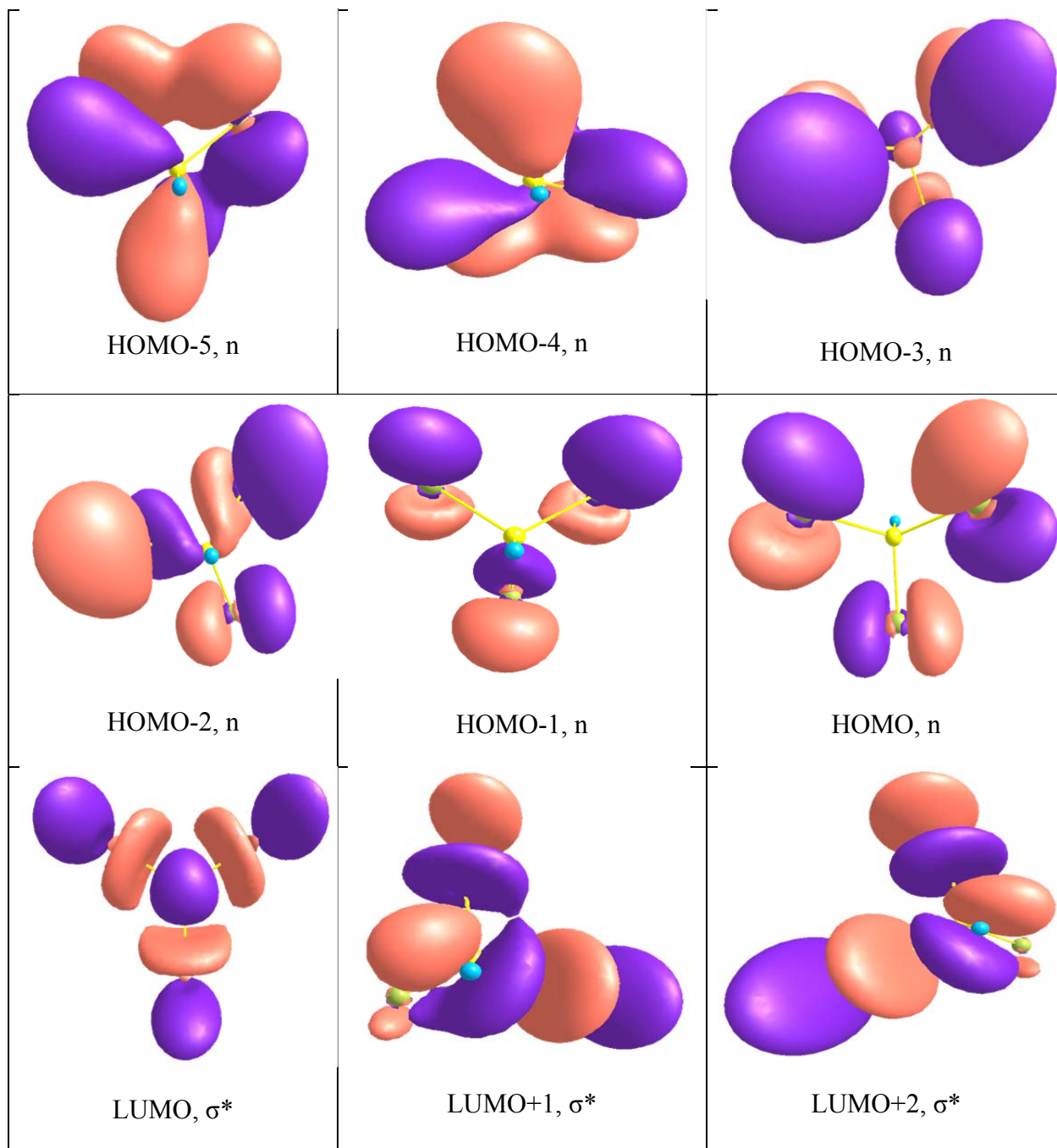
	Geometrical and Energetic Parameters				Comp. time <sup>b</sup>
	C-I, Å	I-I, Å	C-I-I, deg	VET <sup>a</sup>	
6-311G**	2.14	3.60	35.0	4.11, 4.20	6
ANO-RCC-DZVP	2.15	3.62	32.4	4.34, 4.52	4
ANO-RCC-TZVP	2.14	3.54	32.9	4.08, 4.22	13
ANO-RCC-QZVP	2.14	3.50	34.7	4.03, 4.18	40
EOM-CCSD/ 6-311G**	2.15	3.65	32.0	4.24, 4.50	60
Experiment <sup>4</sup>	2.12 <sup>h,i</sup>	3.569 <sup>h,i</sup>	32.6 <sup>h,i</sup>	3.98, 4.34 <sup>c</sup> 4.02, 4.39 <sup>d</sup> 4.19, 4.49 <sup>e</sup> 3.98, 4.36 <sup>f</sup> 3.97, 4.35 <sup>g</sup>	-

<sup>a</sup> Computed vertical excitation energies expressed in eV, <sup>b</sup> computational time needed to perform a single-point energy calculation (in minutes), <sup>c</sup> in *n*-heptane, ref. [8, 43], <sup>d</sup> in *iso*-octane, ref. [11], <sup>e</sup> in cyclohexane, ref. [9], <sup>f</sup> in the gas phase, ref. [12], <sup>g</sup> in *n*-octane, ref. [10], <sup>h</sup> ref. [44], <sup>i</sup> ref. [45].

**Table 7S.** Spin-orbit coupled vertical excitation energies, oscillator strength and composition of the states at the equilibrium geometry of CH<sub>2</sub>I<sub>2</sub> (C<sub>1</sub> symmetry).

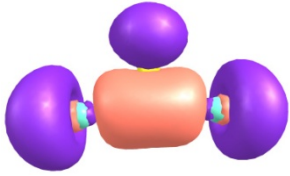
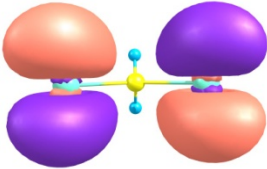
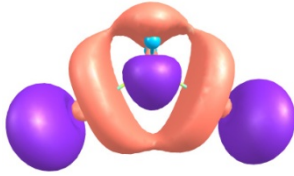
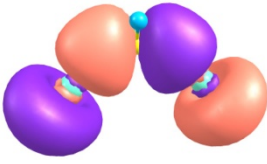
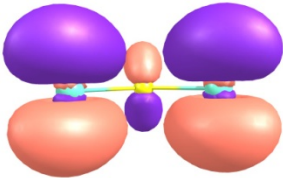
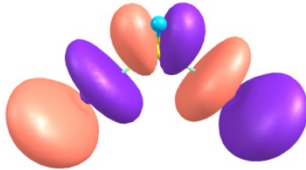
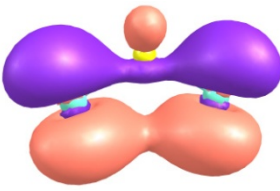
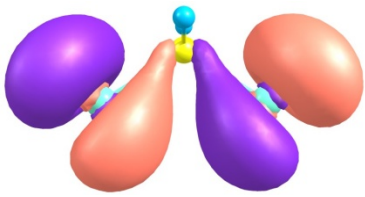
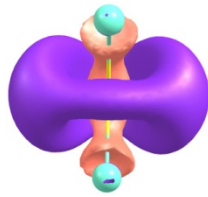
	This work <sup>a</sup>		Ref. [18] <sup>b</sup>	Ref. [19] <sup>c</sup>
0	0	99% 1 <sup>1</sup> A <sub>1</sub>	0, 98.8% 1 <sup>1</sup> A	0, 99% 1 <sup>1</sup> A
1	3.83 (8 10 <sup>-6</sup> )	80% 1 <sup>3</sup> A <sub>1</sub> , 16% 2 <sup>3</sup> A <sub>1</sub>	3.76 (7.90 10 <sup>-7</sup> )	3.858 (5.55 10 <sup>-4</sup> )
2	3.83 (4 10 <sup>-5</sup> )	76% 1 <sup>3</sup> A <sub>1</sub> , 22% 2 <sup>3</sup> A <sub>1</sub>	3.78 (0.0)	
3	3.95 (2 10 <sup>-4</sup> )	90% 1 <sup>3</sup> A <sub>1</sub> , 6% 3 <sup>3</sup> A <sub>1</sub>	3.78 (7.16 10 <sup>-4</sup> )	
4	4.04 (3 10 <sup>-3</sup> )	78% 2 <sup>3</sup> A <sub>1</sub> , 20% 2 <sup>1</sup> A <sub>1</sub> , 2% 3 <sup>1</sup> A <sub>1</sub>	4.03 (1.02 10 <sup>-2</sup> )	4.136 (1.20 10 <sup>-2</sup> )
5	4.38 (2 10 <sup>-6</sup> )	55% 2 <sup>3</sup> A <sub>1</sub> , 35% 3 <sup>3</sup> A <sub>1</sub> , 9% 1 <sup>3</sup> A <sub>1</sub>	4.27 (1.38 10 <sup>-6</sup> )	
6	4.38 (0.0)	40% 3 <sup>3</sup> A <sub>1</sub> , 34% 2 <sup>3</sup> A <sub>1</sub> , 16% 1 <sup>3</sup> A <sub>1</sub>	4.27 (2.94 10 <sup>-7</sup> )	
			4.31 (0.0)	
			4.38 (8.86 10 <sup>-4</sup> )	
			4.50 (8.86 10 <sup>-4</sup> )	
7	4.40 (1 10 <sup>-2</sup> )	40% 3 <sup>3</sup> A <sub>1</sub> , 34% 2 <sup>3</sup> A <sub>1</sub> , 16% 1 <sup>3</sup> A <sub>1</sub>	4.60 (1.25 10 <sup>-2</sup> )	4.207 (4.22 10 <sup>-2</sup> )

<sup>a</sup> MS-CASPT2/CASSI-SO/6-311G\*\*, vertical excitation energies (in eV), oscillator strength (in parentheses) the composition of the spin-coupled states, this work, <sup>b</sup> MS-CASPT2/CASSI-SO/L3//CASPT2L1, calculated vertical excitation energies (in eV) and oscillator strength (in parentheses). The composition of the excited states (in the order of increased energy): 73.6% 1<sup>3</sup>A, 16.6% 2A, 9.7% 3A (state 1), 78.8% 1<sup>3</sup>A, 18.0% 2A, 3.4% 3A (state 2), 81.9% 1<sup>3</sup>A, 10.8% 2A, 7.3% 3A (state 3), 42.5% 2<sup>1</sup>A, 34.9% 2A, 22.6% 3A (state 4), 53.5% 2<sup>3</sup>A, 43.2% 3A, 3.7% 2A (state 5), 63.8% 2<sup>3</sup>A, 33.2% 2A (state 6), 80.6 % 2<sup>3</sup>A, 14.8 % 1A, 4.5% 4A (state 7), 85.2% 2<sup>3</sup>A, 8.8% 3A, 6.0% 2A (state 8), 56.6% 2<sup>3</sup>A, 22.8% 1A, 19.40% 2A (state 9), 54.2% 1<sup>3</sup>A, 34.2% 3A, 11.6% 2A (state 10), <sup>c</sup> MRCI-F12+Q/cc-pVQZ-F12, calculated vertical excitation energies (in eV) and oscillator strength (in parentheses). The composition of the excited states with large oscillator strength (in the order of increased energy): 64% 1<sup>3</sup>B<sub>2</sub>, 23% 1<sup>3</sup>A<sub>2</sub>, 11% 2<sup>1</sup>A<sub>1</sub> (state 2<sup>19</sup>), 82% 2<sup>1</sup>A<sub>1</sub>, 10% 1<sup>3</sup>B<sub>2</sub> (state 4<sup>19</sup>), 69% 3<sup>1</sup>A<sub>1</sub>, 14% 2<sup>3</sup>B<sub>2</sub>, 9% 2<sup>3</sup>A<sub>2</sub> (state 7<sup>19</sup>). The oscillator strength values calculated as  $f = 2/3 |\text{TDM}|^2 \Delta E$  based on the reported<sup>19</sup> VET energies ( $\Delta E$ ) and transient dipole moments (TDM).



**Fig. 5S.** The active space molecular orbitals of  $\text{CHBr}_3$  used for the MS-CASPT2 calculations.



		
HOMO-5, n	HOMO-2, n	LUMO, $\sigma^*$
		
HOMO-4, $\sigma$	HOMO-1, n	LUMO+1, $\sigma^*$
		
HOMO-3, n	HOMO, n	LUMO+2, $\sigma^*$

**Fig. 6S.** The active space molecular orbitals of  $\text{CH}_2\text{I}_2$  used for the MS-CASPT2 calculations.

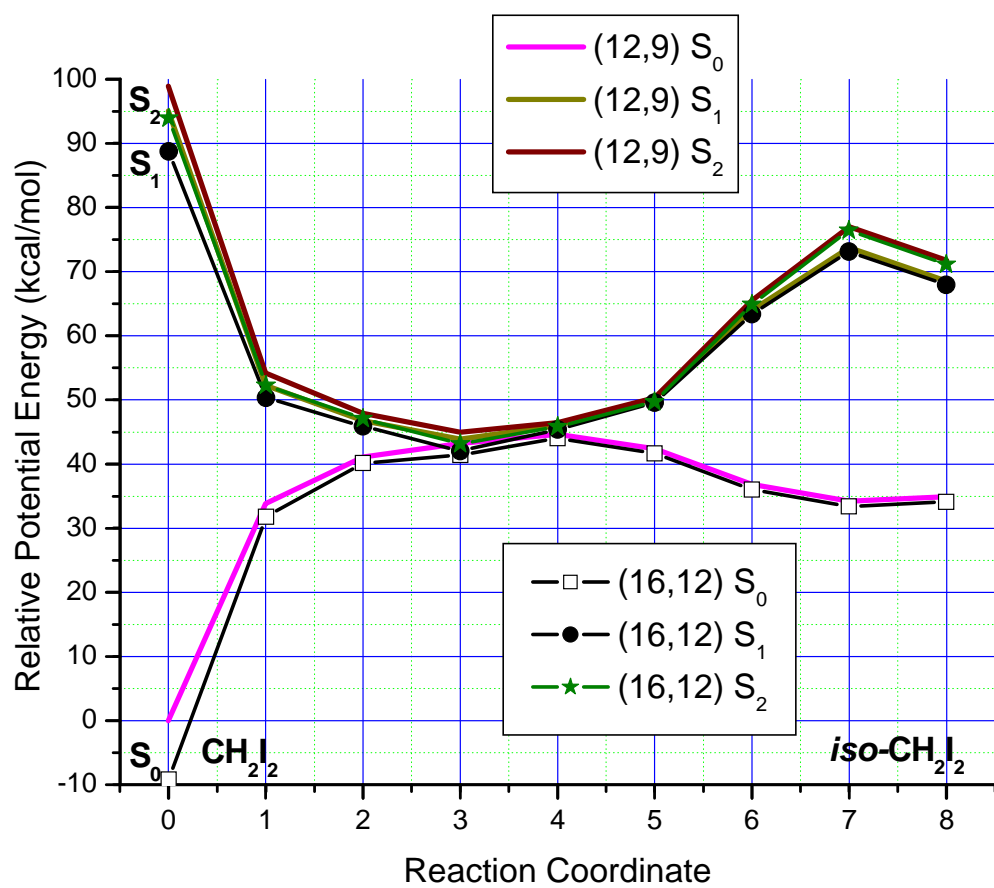


**Fig. 7S.** The effect of the larger active space on the  $CH_2I_2$  MS-CASPT2 MEP.

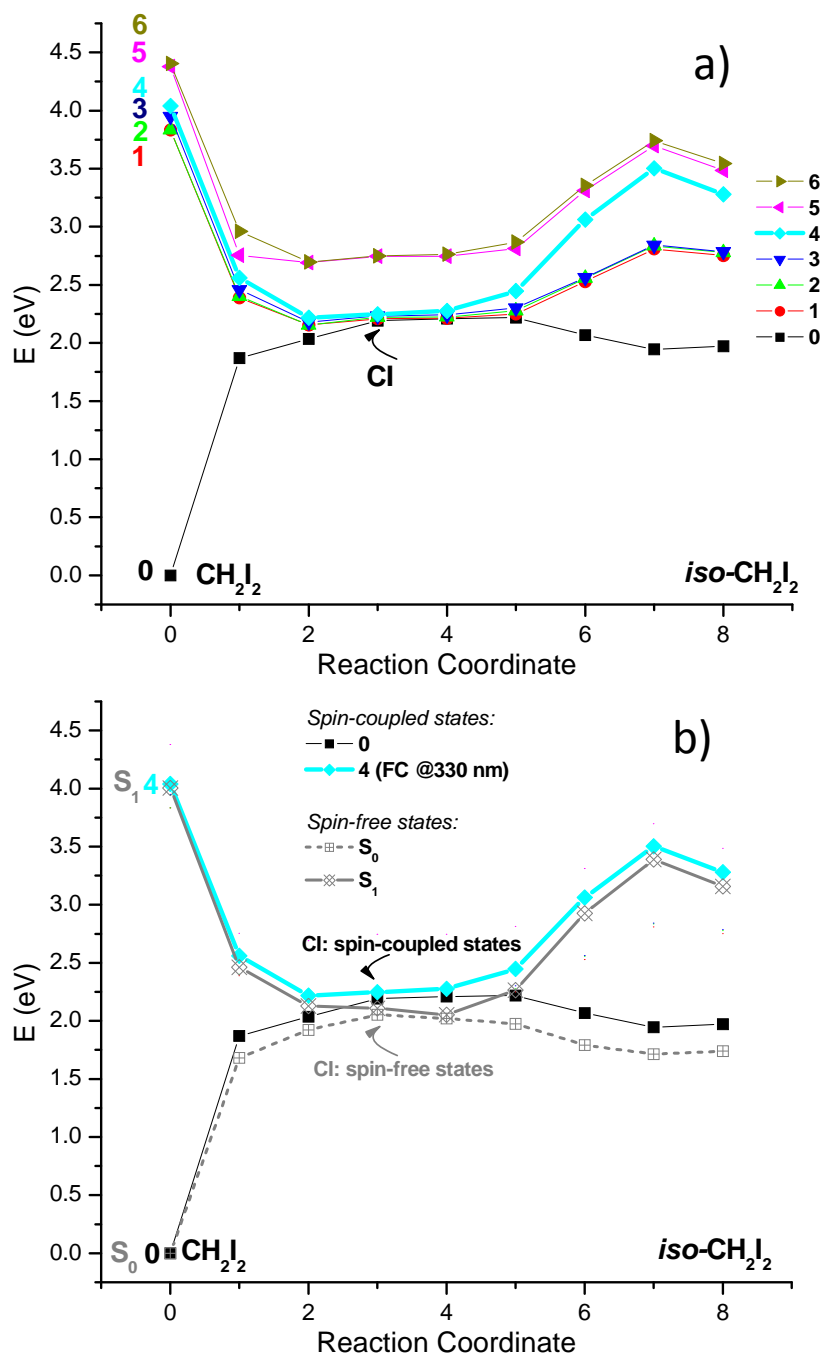


**Fig. 8S.**  $\text{CH}_2\text{I}_2$ : the cut through the spin-orbit-coupled MS-CASPT2/CASSI-SO potential energy surface along the photochemical MEP (panel a, see Table 7S for numbering of the states) and the comparison of the behaviour of the spin-free  $S_0$  and  $S_1$  states and the corresponding spin-orbit-coupled states (panel b).

## References

- (1) K. A. Peterson and J. S. Francisco, *J. Chem. Phys.* 2002, **117**, 6103-6107.
- (2) P. Zou, J. Shu, T. J. Sears, G. E. Hall and S. W. North, *J. Phys. Chem. A* 2004, **108**, 1482-1488.
- (3) D. Xu, J. S. Francisco, J. Huang and W. M. Jackson, *J. Chem. Phys.* 2002, **117**, 2578-2585.
- (4) H.-Y. Huang, W.-T. Chung, R. C. Sharma, C.-Y. Hsu, K.-C. Lin and C.-H. Hu, *J. Chem. Phys.* 2004, **121**, 5253-5260.
- (5) K. D. Bayes, D.W. Toohey, R. R. Friedl and S. P. Sander, *J. Geophys. Res.* 2003, **108**, 4095, doi:10.1029/2002JD002877, D3.
- (6) K.-C. Lin and P.-Y. Tsai, *Phys. Chem. Chem. Phys.* 2014, **16**, 7184-7198.
- (7) Y. Tang, L. Ji, B. Tang, R. Zhu, S. Zhang and B. Zhang, *Chem. Phys. Lett.* 2004, **392**, 493-497.
- (8) M. Kawasaki, S. J. Lee and R. Bersohn, *J. Chem. Phys.* 1975, **65**, 809-814.
- (9) A. Gedanken and M. D. Rowe, *Chem. Phys.* 1979, **36**, 181-186.
- (10) J. Zhang and D. G. Imre, *J. Chem. Phys.* 1988, **89**, 309-313.
- (11) M. Ito, P.-K. Huang and E. M. Kosower, *Trans. Faraday Soc.* 1961, **57**, 1662-1673.
- (12) S. L. Baughcum and S. R. Leone, *J. Chem. Phys.* 1980, **72**, 6531-6545.
- (13) J. B. Koffend and S. R. Leone, *Chem. Phys. Lett.* 1981, **81**, 136-141.
- (14) T. F. Hunter and K. S. Kristjansson, *Chem. Phys. Lett.* 1982, **90**, 35-40.
- (15) K.-W. Jung, T. S. Ahmadi and M. A. El-Sayed, *Bull. Korean Chem. Soc.* 1997, **18**, 1274-1280.
- (16) H. Xu, Y. Guo, S. Liu, X. Ma, D. Dai and G. Sha, *J. Chem. Phys.* 2002, **117**, 5722-5729.
- (17) J. C. Williamson, J. Cao, H. Ihee, H. Frey and A. H. Zewail, *Nature* 1997, **367**, 159-162.
- (18) Ya-J. Liu, L. de Vico, R. Lindh and W.-H. Fang, *ChemPhysChem*. 2007, **8**, 890-898.
- (19) B. W. Toulson, J. P. Alaniz, J. G. Hill and C. Murray, *Phys. Chem. Chem. Phys.* 2016, **18**, 11091-11103.
- (20) H. Schulz, H. Schuler, T. Engers and D. von der Linde, *IEEE Quant Electron* 1989, **25**, 2580-2585.
- (21) B. Dietzej, A. Yartsev and A. N. Tarnovsky *J. Phys. Chem. B* 2007, **111**, 4520-4526.

- (22) A. N. Tarnovsky, V. Sundström, E. Åkesson and T. Pascher, *J. Phys. Chem. A* 2004, **108**, 237-249. Additions/corrections: *ibid.* 2005, **109**, 954–954.
- (23) A. N. Tarnovsky, J.-L. Alvarez, A. P. Yartsev, V. Sundström and E. Åkesson *Chem. Phys. Lett.* 1999, **312**, 121-130.
- (24) S. K. Pal, A. S. Mereshchenko, E. V. Butaeva, P. Z. El-Khoury and A. N. Tarnovsky, *J. Chem. Phys.* 2013, **138**, 124501.
- (25) A. S. Mereshchenko, E. V. Butaeva, V. A. Borin, A. Eyzips and A. N. Tarnovsky, *Nature Chem.* 2015, **7**, 562-568.
- (26) The description of configuration interaction is based on the expansion of the wavefunction in a set of Slater determinants each of which corresponds to a specific excitation of the ground state electronic configuration. The Slater determinant from which the excitations are performed is called reference function. If the excitations are performed from a single Slater determinant, the methods are called single-reference. If the excitations are performed from a linear combination of a number of Slater determinants, the corresponding methods are called multireference.
- (27) P. A. Pulay, *Int. J. Quant. Chem.* 2011, **111**, 3273-3279.
- (28) D. R. Sanjuan, F. Aquilante and R. Lindh, *Comp. Mol. Sci.* 2012, **2**, 585-603.
- (29) R. J. Bartlett and M. Musial, *Rev. Mod. Phys.* 2007, **79**, 291-352.
- (30) J. A. Pople, R. Seeger and R. Krishnan, *Int. J. Quantum Chem.* 1977, **12**, 149-63.
- (31) K. Raghavachari, H. B. Schlegel and J. A. Pople, *J. Chem. Phys.* 1980, **72**, 4654-4655.
- (32) K. Raghavachari and J. A. Pople, *Int. J. Quantum Chem.* 1981, **20**, 1067-1071.
- (33) X. Li and J. Paldus, *Adv. Chem. Phys.* 1999, **110**, 2844-2852.
- (34) R. J. Gdanitz and R. Ahlrichs, *Chem. Phys. Lett.* 1988, **143**, 413-420.
- (35) M. N. Glukhovstev, M. P. McGrath and L. J. Radom, *Chem. Phys.* 1995, **103**, 1878-1885.
- (36) B. O Roos, R. Lindh, P.-Å. Malmqvist, V. Veryazov and P.-O. Widmark, *J. Phys. Chem. A* 2004, **108**, 2851-2858.
- (37) G. Maier, H. P. Reisenauer, J. Hu, L. J. Schaad and B. A. Hess, Jr. *J. Am. Chem. Soc.* 1990, **112**, 5117-5122.
- (38) G. Maier and H. P. Reisenauer, *Angew. Chem. Int. Ed. Engl.* 1986, **25**, 819-822.
- (39) S. A. Reid, *Int. Rev. Phys. Chem.* 2014, **33**, 341-370.
- (40) L. George, A. Kalume, B. J. Esselman, J. Wagner, R. J. McMahon and S. Reid, *J. Chem. Phys.* 2011, **135**, 124503/1-8.

- (41) L. George, A. Kalume, S. A. Reid, B. J. Esselman and R. J. McMahon, *J. Mol. Str.* 2012, **1025**, 61-68.
- (42) F. Abou-Chahine, T. J. Preston, G. T. Dunning, A. J. Orr-Ewing, G. M. Greetham, I. P. Clark, M. Towrie and S. A. Reid, *J. Phys. Chem. A* 2013, **117**, 13388-13398.
- (43) K. Kimura and S. Nagakura, *Spectrochim. Acta* 1961, **17** 166-183.
- (44) O. Hassel, and O. Viervoll, *Acta Chem. Scand.* 1947, **1**, 149-168.
- (45) S. A. Kudchadker and A. P. Kudchadker, *J. Phys. Chem. Ref. Data* 1975, **4**, 457-469.